NANO · MICRO small
www.small-journal.com

Tough Bonding of Liquid Metal-Elastomer Composites for Multifunctional Adhesives

*Tyler A. Pozarycki, Dohgyu Hwang, Edward J. Barron III, Brittan T. Wilcox, Ravi Tutika, and Michael D. Bartlett**

Liquid metal (LM) composites, which consist of LM droplets dispersed in highly deformable elastomers, have recently gained interest as a multifunctional material for soft robotics and electronics. The incorporation of LM into elastic solids allows for unique combinations of material properties such as high stretchability with thermal and electrical conductivity comparable to metals. However, it is currently a challenge to incorporate LM composites into integrated systems consisting of diverse materials and components due to a lack of adhesion control. Here, a chemical anchoring methodology to increase adhesion of LM composites to diverse substrates is presented. The fracture energy increases up to 100× relative to untreated surfaces, with values reaching up to 7800 J m^{-2}. Furthermore, the fracture energy, tensile modulus, and thermal conductivity can be tuned together by controlling the microstructure of LM composites. Finally, the bonding technique is used to integrate LM composites with functional electronic components without encapsulation or clamping, allowing for extreme deformations while maintaining exceptional thermal and electrical conductivity. These findings can accelerate the adoption of LM composites into complex soft robotic and electronic systems where strong, reliable bonding between diverse materials and components is required.

1. Introduction

Soft materials with high stretchability, conformability, and thermal and electrical conductivity are critical for emerging applications in soft robotics and electronics systems.[1–8] Recently, soft composites consisting of liquid metal (LM) droplets dispersed in highly deformable elastomers have gained particular interest, as these materials are soft and stretchable yet display exceptional mechanical, thermal, and electrical properties.[9–19] For example, LM composites can act as soft wiring for wearable devices, yet be flexible enough to seamlessly interface with the contours of human tissue.[20–24] Liquid metal and LM composites are also useful as thermal interface materials (TIMs) for electronic components to improve heat dissipation.[14,25–28] To fully utilize LM composites for applications in soft robotics, wearable computing, and reconfigurable systems, they must be integrated with and attached to different components and interfaces. However, current integration strategies rely primarily on physical attachment, clamping, and encapsulation,[9,15,29,30] and strategies to strongly bond LM composites to diverse materials are lacking.

Bonding LM composites to substrates, particularly polymers, is challenging due to their low surface energy and lack of functional groups.[31–34] One method is to utilize substrates with fibrous or porous structures to allow for mechanical interlocking between the elastomer and substrate.[35,36] However, in many cases, bonding to smooth substrates is desired. Another approach is to perform plasma treatment on the materials for surface cleaning and activation. Plasma bonding is a common technique for adhering silicone elastomers such as PDMS to various surfaces,[37,38] yet there are limitations to the effectiveness of the technique when used with silicones of high plasticizer content. For example, commercial silicones such as Ecoflex are widely used for LM composites and other applications in soft electronics and soft robotics, but their high content of silicone oils leads to challenges with plasma bonding.[31] Silicone surfaces treated with oxygen plasma experience hydrophobic recovery over time due to surface fouling with contaminants and diffusion of unreacted oligomer to the surface, both of which decrease bonding capabilities shortly after treatment.[32] One way to overcome limited work time is to incorporate chemical treatment across interfaces. For example, substrates can be coated with chemical primers such as cyanoacrylates to allow for strong bonding with other materials.[39–41] However, hardened cyanoacrylates

T. A. Pozarycki, D. Hwang, E. J. Barron III, B. T. Wilcox, R. Tutika, M. D. Bartlett
Mechanical Engineering
Soft Materials and Structures Lab
Virginia Tech, Blacksburg, VA 24061, USA
E-mail: mbartlett@vt.edu

D. Hwang, E. J. Barron III, R. Tutika, M. D. Bartlett
Macromolecules Innovation Institute
Virginia Tech, Blacksburg, VA 24061, USA

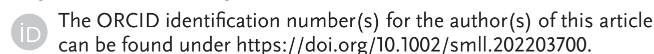
The ORCID identification number(s) for the author(s) of this article can be found under https://doi.org/10.1002/smll.202203700.

© 2022 The Authors. Small published by Wiley-VCH GmbH. This is an open access article under the terms of the Creative Commons Attribution License, which permits use, distribution and reproduction in any medium, provided the original work is properly cited.

DOI: 10.1002/smll.202203700

can generate a mechanical compliance mismatch with deformable materials, resulting in significant stress concentrations and interfacial failures. One promising approach to solve this problem is to treat desired surfaces with functional silanes before bonding.[42] Silane treatment of a material alters its surface chemistry, thus avoiding compliance mismatches generated by the addition of adhesive materials at interfaces. The organosilane (3-aminopropyl)triethoxysilane (APTES) has demonstrated the ability to create stable siloxane bonds between silicones and hydroxylated substrates.[43–45] However, there is limited work on bonding LM composites through surface treatments and to silane-functionalized surfaces.

Here we show an approach to generate tough, permanent adhesion of LM composites to diverse substrates. Strong bonding is achieved by chemically anchoring LM composites to various materials through a surface treatment process that uses oxygen plasma and APTES (**Figure 1**a). This approach increases the fracture energy (G_c) of peel specimens by up to 100× relative to specimens with no treatment (Figure 1b,c), with maximum values around 7800 J m^{-2}. Furthermore, the adhesives can bear heavy loads, as demonstrated by suspending three bricks (total mass 6.8 kg) from a pre-cracked peel specimen with a width of 15 mm (Figure 1d). It is found that by varying LM droplet size from 2–60 µm and volume loading from 20–60%, the fracture energy can be tuned with tensile modulus and thermal conductivity. These results show that the smallest droplets lead to the highest values of G_c and modulus, while thermal conductivity is similar over different size droplets, thus demonstrating control of toughness and thermal properties. Finally, we demonstrate potential applications of this tough bonding approach in soft robotics and electronics by chemically anchoring rigid materials and electronic components to LM composite to create robust soft electronics systems. These systems are developed without encapsulation or clamping of the LM composite, thus simplifying integration while maintaining extreme deformability and exceptional thermal and electrical performance.

2. Results and Discussion

The LM composites consist of Ecoflex silicone elastomer with dispersed droplets of eutectic gallium–indium (EGaIn).

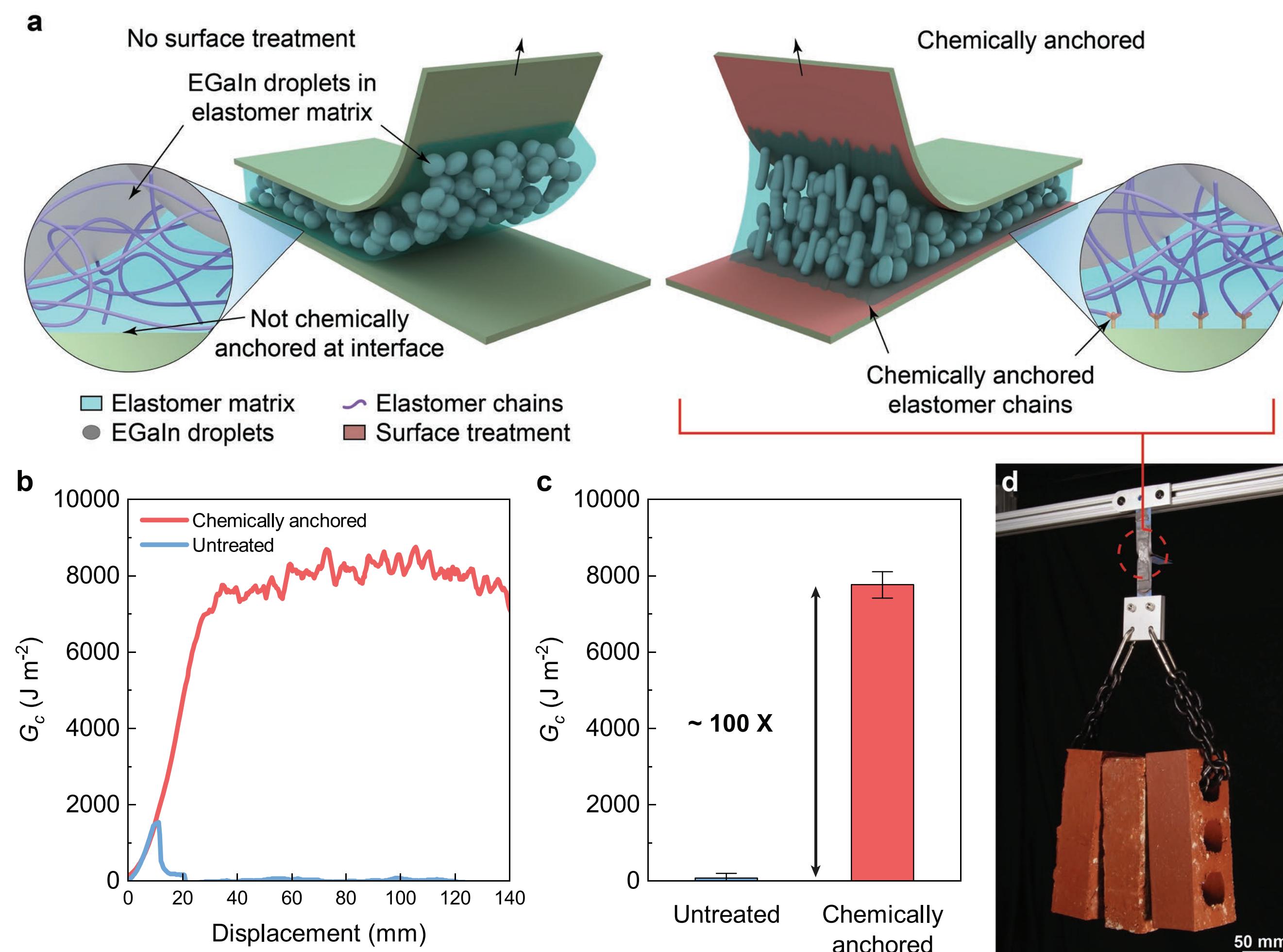

Figure 1. Strong bonding of liquid metal composite. a) Schematic representation of liquid metal composite adhesion without (left) and with (right) chemical anchoring. b) Fracture energy (G_c) versus displacement of representative LM composites ($\phi = 20\%$, $d = 2$ µm) undergoing peeling. c) Fracture energies of untreated and chemically anchored samples ($\phi = 20\%$, $d = 2$ µm). Error bars represent the standard deviation for $n = 3$. d) Strong LM composite adhesive supporting bricks of total mass 6.8 kg from a 15 mm wide, pre-cracked peel specimen.

© 2022 The Authors. Small published by Wiley-VCH GmbH

The volume fraction of LM was varied from $0 \leq \phi \leq 60\%$ with droplet sizes ranging from $2 \leq d \leq 60\,\mu m$ based on particle analysis (see Figures S1 and S2, Supporting Information). To create chemically anchored samples, substrates were treated with oxygen plasma, submerged into a 0.1 vol% APTES in ethanol solution, and allowed to dry at room temperature. Then, liquid-state LM composite was cast onto the surface and cured. Untreated samples were prepared using a similar procedure except oxygen plasma and APTES solution were not utilized (see experimental section for more details). The APTES creates an abundance of functional amine groups on a material surface. Additionally, pretreating with plasma increases the amount of active sites for APTES to attach compared to a pristine material.[46,47] Upon casting liquid-state LM composite onto the treated surface, chemical anchoring of elastomer chains occurs through interfacial compatibilization of the silane treatment and the silicone elastomer, which can occur through the formation of an interpenetrating polymer network between polymer chains and the silane molecules (Figure 1a).[48]

Adhesion performance was analyzed by conducting T-peel tests in which LM composite was cast between two flexible polyethylene terephthalate (PET) adherends (**Figure 2**a). The untreated samples experienced adhesive failure at the composite-PET interface. In contrast, the chemically anchored composites did not debond from the adherends. Instead, the crack propagated cohesively through the composite, as material fracture was more energetically favorable than breaking the interfacial bonds. To investigate LM composite fracture on the microscale, the crack front of a chemically anchored sample was monitored during peeling (Figure 2b–d). We observed significant deformation which resulted in the LM inclusions elongating in the damage region. This behavior is represented schematically in Figure 2e and highlights the reconfigurable nature of the LM droplets under deformation.

2.1. Effects of LM Microstructure on Fracture Energy

To investigate the effect of microstructure on fracture energy, nine distinct compositions of chemically anchored composites were tested under T-peel, including three LM volume loadings ($\phi = 20\%$, 40% , 60%) each with three mean droplet diameters (d = 2, 15, and 60 µm). Unloaded Ecoflex samples were also fabricated ($\phi = 0\%$). For each sample, the fracture energy G_c is obtained by normalizing the measured plateau peel force F by the composite width w, $G_c = 2F/w$.[49,50] A decrease in volume fraction and mean droplet diameter is observed to lead to an increase in fracture energy (**Figure 3**a). The largest G_c is obtained with $\phi = 20\%$, $d = 2$ µm, which is similar to that of the unfilled elastomer. Although G_c decreases with increasing ϕ, a significant G_c value of 2880 ± 150 J m^{-2} is achieved for $\phi = 60\%$. Previous work by Kazem et al. has shown that higher LM volume fractions in soft elastomers result in an extreme toughening effect;[51] however, the work presented here shows a contrasting trend which is attributed to differences in the crack propagation mechanism. Kazem et al. showed that extreme toughening is a result of crack redirection due to elongation of LM inclusions perpendicular to the propagating crack. In this work, chemically anchored specimens tended to fracture in a serrated or sawtooth pattern, where the pronouncement of the pattern has been shown to depend on parameters such as loading conditions, sample thickness, and adherend thickness.[52,53] This characteristic serrated morphology likely results in the crack moving back and forth along the direction of loading, not directly through the centerline of the crack front. This would reduce the crack deflection effectiveness of the LM droplets, allowing the crack to propagate along the inclusions, not through the inclusions where deflection could occur. Next, with regard to LM droplet size, smaller LM droplets tend to act as stiffer inclusions.[54] This has been shown through elastocapillary arguments as well as the existence of a stiff, solid oxide layer on the surface of LM particles.[55] As LM droplet size

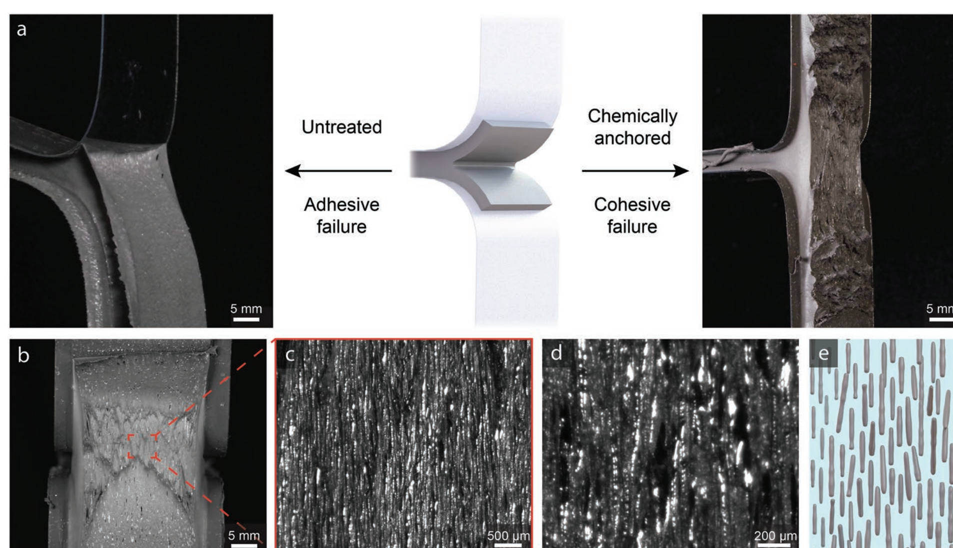

Figure 2. LM composite adhesion. a) Adhesive and cohesive failures of LM composite sample ($\phi = 20\%$, $d = 2$ µm) in T-peel without and with APTES surface treatment. b) Macrophotograph of the crack front of an LM adhesive ($\phi = 20\%$, $d = 60$ µm) undergoing cohesive fracture with c,d) showing the corresponding micrographs. e) Schematic representation of liquid metal droplet elongation at the crack front.

© 2022 The Authors. Small published by Wiley-VCH GmbH

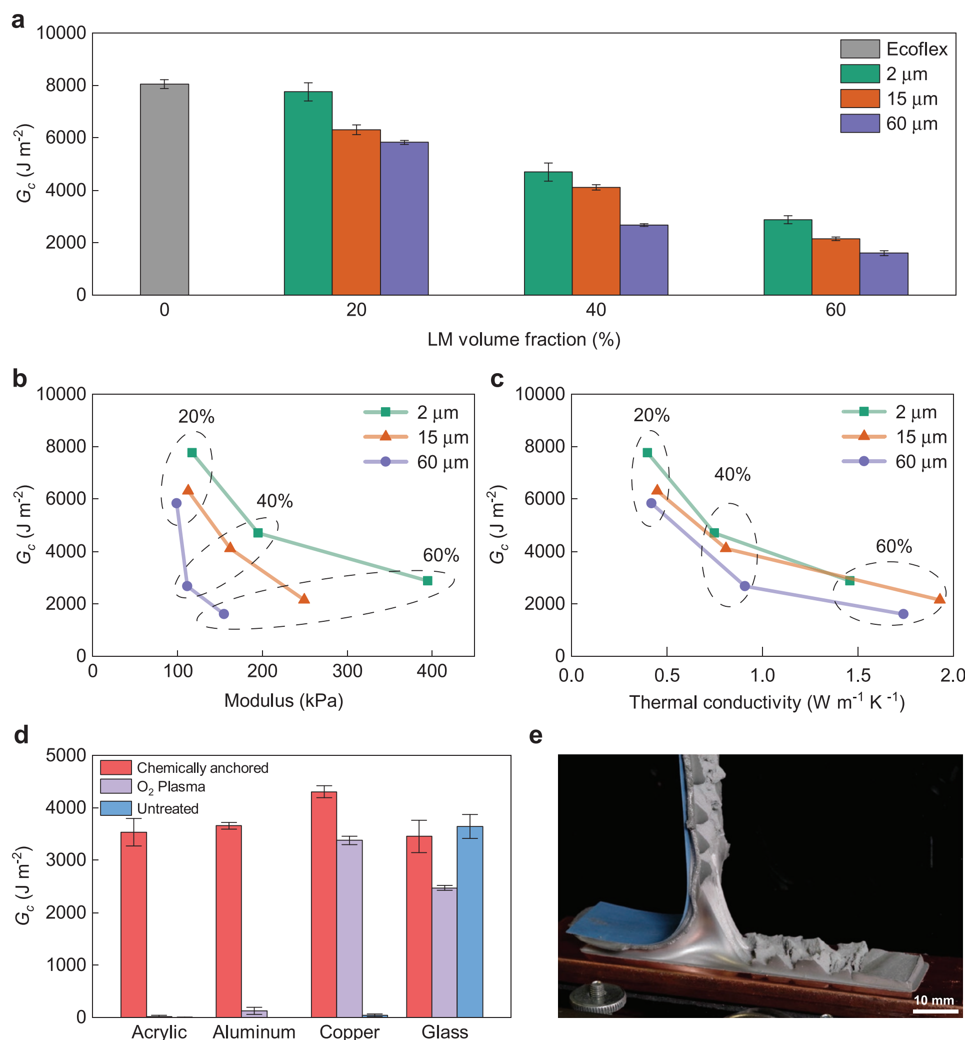

Figure 3. Adhesion and property characterization of LM composites. a) Fracture energies of LM composites in T-peel. b) Comparison of LM composite fracture energy and elastic modulus. c) Comparison of LM composite fracture energy and thermal conductivity. d) Fracture energy of LM composite on varied surfaces in 90° peel for $\phi = 40\%$, $d = 15$ µm. e) Macrophotograph of the cohesive failure of a 90° peel sample on copper. Error bars represent the standard deviation for $n = 3$.

decreases, the ratio of outer solid surface area to inner liquid volume increases, resulting in a higher effective stiffness. This trend is similar to elastocapillarity, which states that the surface tension of liquid inclusions will stiffen a composite when the inclusion size is sufficiently small. This increased composite stiffness tends to toughen the LM composites for the same ϕ as observed in Figure 3a.

The effect of LM droplets on composite modulus and thermal conductivity are important areas of research for soft matter systems.[13] Previous work has focused on understanding the effect of LM droplets on the mechanical response of soft composites.[10] Additionally, significant research has been performed to create LM composites with exceptional thermal conductivities (k), which can be achieved through high liquid metal content for isotropic composites (k = 2–6.7 W m^{-1} K^{-1}),[56,57] or by droplet elongation to increase functionality in the direction of alignment (k = 3.8–13.0 W m^{-1} K^{-1}).[9,14,26] These materials can benefit from simplified integration through tough bonding; however, the relationship between fracture energy with thermal conductivity and tensile modulus has not been explored.

In this work, we show LM composites with desirable thermal and mechanical properties while also achieving tough adhesion to various substrates. Figure 3b shows the relationship between G_c and composite modulus. By controlling the volume loading and mean LM droplet diameter, composites with prescribed combinations of toughness and modulus can be created. For example, by maintaining an LM volume fraction of 20% and changing the mean droplet diameter from 2 to 60 µm, the fracture energy can be tuned by ≈2000 J m^{-2} with a slight change in modulus of less than 20 kPa. In contrast, at higher LM volume fractions, the mean LM droplet diameter is shown to have a greater effect on modulus than on toughness. At a volume fraction of 60%, a change in modulus of over 240 kPa results in a change in G_c of 1275 J m^{-2} as mean droplet diameter is changed from 2 to 60 µm.

© 2022 The Authors. Small published by Wiley-VCH GmbH

The thermal conductivity of these composites can also be tuned while controlling the fracture energy. Figure 3c shows the relationship between G_c and k, where G_c generally decreases with increasing composite thermal conductivity. The thermal conductivity does not display a pronounced dependence on LM droplet diameter, and instead is dependent on volume fraction. In contrast, changes in droplet size have a noticeable effect on fracture energy. These findings are enabling for the development of LM composite adhesives with desired combinations of thermal conductivity and fracture energy, which can be controlled by LM volume fraction and droplet size, respectively.

2.2. Robust Adhesion to Multiple Surfaces

Strong bonding to diverse substrates is required for a variety of applications. In order to show the broad application of the chemical anchoring technique, one composition of LM composite (ϕ = 40%, d = 15 µm) is bonded to several rigid, nonporous substrates. The fracture energy is then measured via 90° peel test, for which $G_c = F/w$ (Figure 3d). All untreated samples, except for glass, experience adhesive failure at the composite-substrate interface. This results in very low adhesion (<10 J m^{-2} for acrylic and aluminum and <50 J m^{-2} for copper), as is commonly observed with silicones and LM composites. Oxygen plasma treatment without APTES was also performed, where only selected substrates showed strong adhesion such as copper and glass, while acrylic and aluminum showed low adhesion. In contrast, all chemically anchored samples that utilize both oxygen plasma and APTES treatment fracture through the composite thickness with G_c values over 3000 J m^{-2}. It is observed that the cohesive fracture energy measured in 90° peel for the chosen sample composition is similar to that measured in T-peel. Furthermore, samples tested in 90° peel also display a serrated or sawtooth appearance of the fracture surface (Figure 3e). Given these results, the chemical anchoring technique is promising for the incorporation of LM composites into larger systems consisting of diverse materials.

2.3. Integration of LM Composites into Electronic Systems

The high thermal conductivity of LM composite gives rise to its potential use as a thermal interface material in modern electronics.[14,27,58] Furthermore, an electrically insulating matrix such as Ecoflex lessens the risk of electrical shorting, mitigates the corrosive effect of gallium,[26,59] and allows for chemical anchoring techniques to be leveraged. To demonstrate, computer graphics benchmark tests are conducted using the as-received thermal compound between the graphics processing unit (GPU) and a passive heatsink. The compound is then replaced with chemically anchored LM composite (ϕ = 60%, d = 60 µm) and unfilled Ecoflex. It is found that the GPU temperature and performance with LM composite is similar to the stock thermal compound (**Figure 4**a,b). However, Ecoflex performs notably worse, as the GPU reaches much higher temperatures. Finally, to demonstrate strong adhesion from chemical anchoring, the screws holding the heatsink (66 g) in place on the GPU circuit board are removed and an additional 50 g mass is suspended near the 7.6 × 9 mm area containing the chemically anchored LM composite (Figure 4c). The strong adhesion and thermal control of the LM composite could be leveraged for future integrated systems within rigid electronics applications.

Along with its high thermal conductivity, LM composite demonstrates exceptional stretchability and toughness, and these properties are especially important to the emerging field of stretchable electronics. To demonstrate a stretchable electronics system which leverages all three properties, an LM composite sample is created in which electronic components and external leads are directly integrated without encapsulation or clamping (Movie S1, Supporting Information). Here, a high-power LED (Cree Extreme High Power (XHP)) and external copper

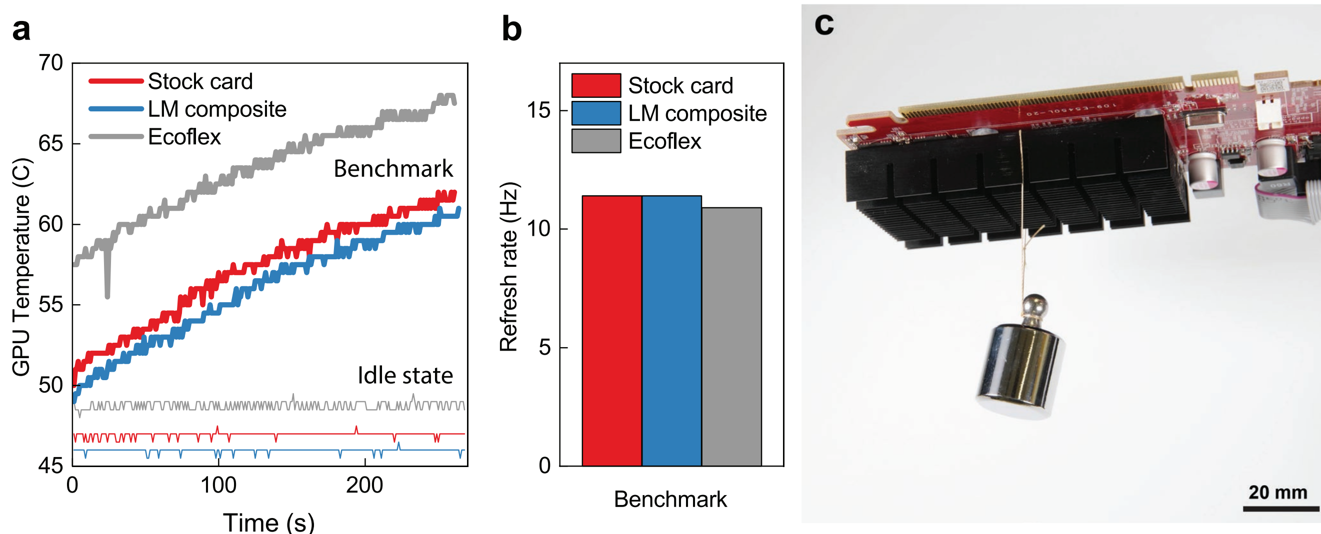

Figure 4. Integration and heat dissipation of electronics with LM composites. a) Temperature measured by the GPU thermocouple during idle and benchmark tests. b) Performance of the graphics card with the stock configuration and with LM composite and Ecoflex as replacements for the thermal interface material. c) Suspension of both the heatsink (66 g) and an additional 50 g from a chemically anchored LM composite.

© 2022 The Authors. Small published by Wiley-VCH GmbH

contacts are chemically anchored to an LM composite sample ($\phi = 60\%$, $d = 60$ µm). A pristine Ecoflex sample is also created with untreated copper contacts (**Figure 5**a). On both samples, LM traces are spray coated from the copper to the LED contacts to complete an electrically conductive network. The LEDs are supplied with a current of 0.6 A while the samples remain unstretched, resulting in a power output of ≈3 W with a high brightness. After 80 s, the LED anchored to the Ecoflex sample reaches a temperature over 135 °C, leading to thermal failure (Figure 5b,c(i,ii)). The LED anchored to the composite reaches a temperature of ≈85 °C and remains on after the same amount of time (Figure 5b,d(i,ii)). At this point, both the samples are stretched and at ≈35% global strain, the Ecoflex sample completely detaches from the untreated bottom copper contact and the top grip continues to rise (Figure 5c(iii,vi)). In comparison, the LM composite remains anchored to its treated copper contacts until ≈310% global strain, at which the sample fractures at the bottom neck, breaking the LED circuit (Figure 5d(iii,vi)). Thus, chemical anchoring prevents failure due to debonding between components and instead allows for system design based on the mechanical properties of the composite material. Furthermore, LM composite allows for more efficient thermal dissipation, while the pristine polymer demonstrates poor thermal properties.

The use of chemically anchored LM composites in stretchable electronics systems is further demonstrated through the robust attachment of a circular membrane film (750 µm) to an LED and a supporting acrylic substrate, without encapsulation or mechanical clamping (Figure 5e,i). After supplying the LED with 0.05 A current, the system is subjected to tensile and torsional stresses (Movie S2, Supporting Information). During each stress scenario, the film remains bonded to the acrylic substrate and the LED remains on (Figure 5e(ii,iii)). Additionally, the LED does not detach from the composite even when stress concentration occurs across the small interfacial area by pulling the LED with tweezers (Figure 5e(iv)). These characteristics demonstrate the exceptional toughness of the chemically anchored interfaces as well as the ability to leverage the functional properties of LM composites for the creation of robust and stretchable systems.

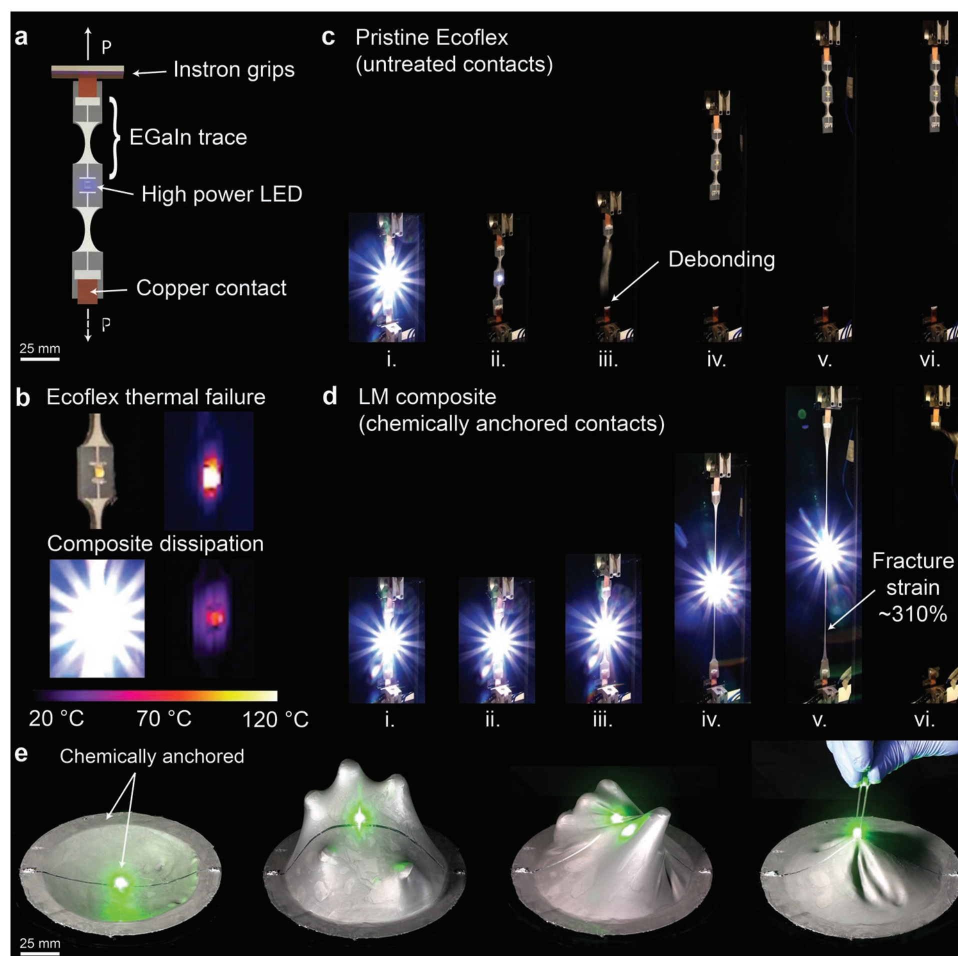

Figure 5. Stretchable circuits through tough LM composite adhesives. a) Schematic representation of an integrated LM composite device. b) Thermal profiles of Ecoflex and LM composite samples after 80 s. c) Ecoflex sample timelapse, showing thermal failure of the LED (ii) and adhesive failure at the bottom copper contact (iii). d) LM composite sample timelapse, showing high stretchability and heat dissipation and eventual fracture through the bottom neck (v,vi) at ≈310% global applied strain. e) LM composite thin film with (from left to right) chemically anchored to an LED and supporting acrylic substrate, hand-stretching, torsion, and stress applied directly to the LED while pulling with tweezers.

© 2022 The Authors. Small published by Wiley-VCH GmbH

3. Conclusions

In this work, we present a method to permanently adhere LM composites to a variety of materials. Tough adhesion is achieved through the functionalization of surfaces with oxygen plasma and APTES, which allows for chemical anchoring of elastomer chains to a desired material. Chemical anchoring leads to steady-state crack propagation in the composite layer, resulting in an increase in fracture energy of up to 100× relative to samples with untreated adherends. The fracture energy is controlled by LM composite microstructural parameters such as droplet size and volume loading. Additionally, G_c demonstrates paired tunability with other functional properties such as modulus and thermal conductivity. Notably, the fracture energy of the toughest composite system ($\phi = 20\%$, $d = 2$ µm) is similar to that of the pristine elastomer ($\phi = 0\%$). Given that smaller values of both ϕ and d tend to translate to higher values of G_c, the fabrication of composites with nanoparticles, volume fractions less than 20%, or a combination thereof may provide opportunities for creating a composite system in which the fracture energy is superior to that of the pristine elastomer. However, the balance of properties such as thermal conductivity and modulus may also need to be considered, allowing for future optimization of desired properties by controlling particle size, LM loading, elastomer choice, and distribution and shape of droplets. These properties are particularly useful for applications in soft electronics and robotics since tough, stretchable, and thermally conductive materials are often desired in these areas. The utility of the bonding method is demonstrated by successfully integrating various materials with LM composites to create robust, highly stretchable, and thermally conductive soft electronics systems. These results could inspire the development of more complex soft matter systems not otherwise possible without reliable bonding, thus creating more seamless integration between soft functional materials and rigid electronic components for robust, hybrid electronic, and robotic systems.

4. Experimental Section

Liquid Metal Composite Fabrication: LM particles were fabricated using an in situ technique where the bulk LM was first added to uncured elastomer (Ecoflex 00-30, Smooth-On, Inc.) and mixed with a stirring rod for 2 min. To achieve particle diameters of 60 and 15 µm, solutions containing 66 vol% LM in elastomer were shear mixed in a dual asymmetric centrifuge (DAC 1200-500 VAC, FlackTek) at 1200 and 1700 RPM, respectively. To fabricate particles with a 2 µm diameter, separate solutions containing 70 vol% LM in prepolymer and LM in curing agent were mixed using an overhead mixer (6015 Ultra Speed, Caframo) at 6000 RPM. Emulsions containing the desired particle sizes were then diluted with uncured elastomer to set the volume loading.[56] In the case of 2 µm particle size, the separate 70 vol% solutions were combined 1:1 and subsequently diluted. The final composites were cast into molds to prepare the samples for testing.

T-Peel Fabrication: PET adherends were laser cut into 125 mm × 20 mm strips from stock sheets of 125 µm-thick PET. After cleaning with isopropyl alcohol, the strips were treated with oxygen plasma (3 min, 300 mTorr oxygen, 400 W, PE-75 Series, Plasma Etch, Inc.) to functionalize the surface in preparation for APTES treatment. The plasma-treated PET strips were then dip coated in a 0.1 vol% APTES in ethanol solution and placed onto a glass plate to dry for 5 h. Ecoflex and LM composite samples were cast directly onto an APTES-treated PET adherend placed underneath a 75 mm × 15 mm × 3.2 mm acrylic mold. A second APTES-treated PET adherend was laid on top of the uncured sample. The completed T-peel specimen was cured at 80 °C for at least 12 h. Viscous composites such as $\phi = 60\%$, $d = 2$ µm were cured at room temperature for 12–15 h and then at 80 °C for 3 h. After curing, the mold was removed and a 10 mm pre-crack was cut through the midplane of the thickness and along the sample length using a razor blade.

90° Peel Fabrication: Substrates were cleaned with isopropyl alcohol, treated with oxygen plasma, submerged into a 0.1 vol% APTES in ethanol solution, and left to dry. An acrylic mold was secured on top of the treated substrate and the LM composite was cast onto the substrate surface. Finally, an APTES-treated PET adherend was placed on top of the uncured sample and the specimen was left to cure at room temperature for at least 12 h. Following room temperature curing, the mold was removed and the sample was cured at 80 °C for 3 h. 90° peel specimens were also given a 10 mm pre-crack prior to testing.

Stretchable Electronics LED Sample Fabrication: Copper strips 60 mm in length (Basic Copper) and LEDs (Cree XLAMP XHP50 GEN 3, Digi-Key Electronics) were cleaned with isopropyl alcohol, treated with oxygen plasma, submerged into a 0.1 vol% APTES in ethanol solution, and left to dry. Two strips were then secured with VHB tape at 25 mm along the length on each side of a 170 mm × 40 mm acrylic backing layer, and the sample mold was then secured on top of this assembly with electrical tape. The sample was cast into the mold and cured at 80 °C for 60–90 min. After curing, the sample was removed from the mold and LM traces were spray coated onto the sample using a stencil made from laser patterned orange mask (Blazer Orange Laser Mask, Johnson Plastics Plus). The LED heat sink was dabbed with uncured sample, placed onto the center of the specimen, and cured at 40 °C for 1 h. After curing, an electrically conductive network was completed by using EGaIn-copper paste to connect the LM traces to the edges of the copper strips and LED leads.

Stretchable Electronics Circular Thin Film Fabrication: An acrylic ring of 155 mm outer diameter and 135 mm inner diameter was laser cut from an acrylic sheet of 3.2 mm thickness. The ring and LED (Luxeon Rebel 530NM SMD, Digi-Key Electronics) were chemically treated using the same process described above. LM composite ($\phi = 60\%$, $d = 60$ µm) was cast onto an acrylic slide coated with mold release (Ease Release 200, Reynolds Advanced Materials) and the thickness was set using a thin film applicator (Zua 2000, Proceq). The film was cured at 80 °C for 30 min. After curing, a circle of 140 mm diameter was laser patterned into the thin film. The acrylic ring was coated with uncured LM composite and placed over top of the circular thin film. This assembly was cured at 80 °C for 12 h. Following this cure, the circular thin film with the chemically anchored ring was removed from the acrylic slide. LM traces were spray coated and the LED was connected to the center of the film using uncured sample. The final assembly was cured at 40 °C for 1 h.

Peel Specimens: T-peel samples were tested under uniaxial tension and 90° peel samples were tested using a wire cable actuated test apparatus on an Instron 5944 universal testing system. T-peel and 90° peel tests were performed at an extension rate of 254 and 60 mm min^{-1}, respectively. Fracture energy was calculated from the plateau region of the load–displacement curve.

Tension Tests: Mechanical properties were measured under uniaxial tension. Dogbone specimens were die-cut according to 50% dimensions of ASTM D412-C specimens. The test was performed at an extension rate of 1 mm s^{-1} using an Instron 5944 universal testing system. Tensile modulus was calculated from the stress–strain curve up to 5% strain.

Thermal Imaging: IR images were captured with a FLIR E54sc infrared camera at a frame rate of 30 frames per second with emissivity = 0.9 and reflection temperature of 20 °C.

Optical Microscopy: Optical micrographs were obtained using a Zeiss Axio Zoom v16 stereo microscope.

Scanning Electron Microscopy: SEM images were obtained on a FEI Quanta 600 FEG-SEM in back-scattered electron (BSE) mode at a spot size of 5.5 and an accelerating voltage of 30 kV. The cross-sections of

© 2022 The Authors. Small published by Wiley-VCH GmbH

samples were sputter coated with a Pt–Pd layer of ≈10 nm thickness prior to SEM analysis.

Particle Analysis: Fiji software was used to perform particle analysis in which the area of a particle was calculated from a binary image and an ellipse of that area was fit on the particle. The mean particle size and standard deviation were calculated from plotting a histogram of the major diameters of the ellipses and utilizing Gaussian and lognormal fits on the data. Micrographs with ellipses fits and corresponding particle size histograms can be referenced in the Supporting Information.

Thermal Conductivity Measurement: Thermal conductivity was measured using a transient hot wire (THW) measurement detailed in previous work.[56]

Graphics Card Performance Benchmarking: The performance of a Visiontek Radeon 5450 graphics card was evaluated by measuring idle temperatures and running Unigine Heaven 4.0 as a benchmark program. The computer was a Dell Precision 5820 Tower X-series with an i9-10900X CPU and 32 GB of RAM. All tests were conducted with the side panel of the computer removed. To measure GPU temperature, the TechPowerup GPU-Z program was used, and "GPU Temp #1" was recorded. To measure the idle temperature, the computer was turned on and GPU-Z tool measured the temperature after steady-state was achieved for at least 10 min. To record the refresh rate, MSI Afterburner with Rivatuner Statistics Server was used. During benchmark testing, the rendered resolution was 1280 × 720 in DirectX 11 mode, and all settings were set to low with tessellation, stereo 3D, multi-monitor, and anti-aliasing disabled. No other processes were conducted on the computer for the duration of the benchmark. After a benchmark run was conducted, the computer was left unused until the GPU temperature returned to its idle state before starting another benchmark run.

Statistical Analysis: The meaning of all error bars was described within the captions of the corresponding figures.

Supporting Information

Supporting Information is available from the Wiley Online Library or from the author.

Acknowledgements

The authors acknowledge support from the Office of Naval Research Young Investigator Program (YIP) (N000142112699), the Defense Advanced Research Projects Agency Young Faculty Award (DARPA YFA) (D18AP00041), and the Institute for Critical Technology and Applied Science (ICTAS) at Virginia Tech. This work was performed in part at the Nanoscale Characterization and Fabrication Laboratory, which is supported by the Virginia Tech National Center for Earth and Environmental Nanotechnology Infrastructure (NanoEarth), a member of the National Nanotechnology Coordinated Infrastructure (NNCI), supported by NSF (ECCS 1542100 and ECCS 2025151). The authors also appreciate discussions with Vince Baranauskas.

Conflict of Interest

The authors declare no conflict of interest.

Author Contributions

T.A.P., D.H., and E.J.B. III contributed equally to this work. T.A., D.H., E.J.B, B.T.W., R.T., and M.D.B. designed research; T.A., D.H., E.J.B, B.T.W., and R.T. performed research; T.A., D.H., E.J.B, B.T.W., R.T., and M.D.B. analyzed data; T.A., D.H., E.J.B, B.T.W., R.T., and M.D.B. wrote the paper.

Data Availability Statement

The data that support the findings of this study are available from the corresponding author upon reasonable request.

Keywords

adhesion, liquid metals, soft composites, soft robotics, stretchable electronics

Received: June 14, 2022
Revised: August 8, 2022
Published online:

[1] D.-H. Kim, N. Lu, R. Ma, Y.-S. Kim, R.-H. Kim, S. Wang, J. Wu, S. M. Won, H. Tao, A. Islam, K. J. Yu, T.-i. Kim, R. Chowdhury, M. Ying, L. Xu, M. Li, H.-J. Chung, H. Keum, M. McCormick, P. Liu, Y.-W. Zhang, F. G. Omenetto, Y. Huang, T. Coleman, J. A. Rogers, *Science* **2011**, *333*, 838.
[2] R. F. Shepherd, F. Ilievski, W. Choi, S. A. Morin, A. A. Stokes, A. D. Mazzeo, X. Chen, M. Wang, G. M. Whitesides, *Proc. Natl. Acad. Sci.* **2011**, *108*, 20400.
[3] A. Tonazzini, S. Mintchev, B. Schubert, B. Mazzolai, J. Shintake, D. Floreano, *Adv. Mater.* **2016**, *28*, 10142.
[4] D. Hwang, E. J. Barron III, A. T. Haque, M. D. Bartlett, *Sci. Rob.* **2022**, *7*, eabg2171.
[5] D. Rus, M. T. Tolley, *Nature* **2015**, *521*, 467.
[6] E. J. Barron III, R. S. Peterson, N. Lazarus, M. D. Bartlett, *ACS Appl. Mater. Interfaces* **2020**, *12*, 50909.
[7] J. Kang, J. B.-H. Tok, Z. Bao, *Nat. Electron.* **2019**, *2*, 144.
[8] Z. J. Farrell, C. J. Thrasher, A. E. Flynn, C. E. Tabor, *ACS Appl. Nano Mater.* **2020**, *3*, 6297.
[9] M. D. Bartlett, N. Kazem, M. J. Powell-Palm, X. Huang, W. Sun, J. A. Malen, C. Majidi, *Proc. Natl. Acad. Sci. U. S. A.* **2017**, *114*, 2143.
[10] G. G. Guymon, M. H. Malakooti, *J. Polym. Sci.* **2022**, *60*, 1300.
[11] C. Majidi, K. Alizadeh, Y. Ohm, A. Silva, M. Tavakoli, *Flexible Printed Electron.* **2022**, *7*, 013002.
[12] M. D. Dickey, *Adv. Mater.* **2017**, *29*, 1606425.
[13] S. Chen, H.-Z. Wang, R.-Q. Zhao, W. Rao, J. Liu, *Matter* **2020**, *2*, 1446.
[14] A. T. Haque, R. Tutika, R. L. Byrum, M. D. Bartlett, *Adv. Funct. Mater.* **2020**, *30*, 2000832.
[15] E. J. Markvicka, M. D. Bartlett, X. Huang, C. Majidi, *Nat. Mater.* **2018**, *17*, 618.
[16] R. Tutika, A. Haque, M. D. Bartlett, *Commun. Mater.* **2021**, *2*, 64.
[17] L. Mou, J. Qi, L. Tang, R. Dong, Y. Xia, Y. Gao, X. Jiang, *Small* **2020**, *16*, 2005336.
[18] S. G. Wallace, N. P. Bradshaw, N. X. Williams, J. H. Qian, K. W. Putz, C. E. Tabor, M. C. Hersam, *Adv. Mater. Technol.* **2021**, *7*, 2101178.
[19] N. Pekas, Q. Zhang, D. Juncker, *J. Micromech. Microeng.* **2012**, *22*, 097001.
[20] P. A. Lopes, D. F. Fernandes, A. F. Silva, D. G. Marques, A. T. de Almeida, C. Majidi, M. Tavakoli, *ACS Appl. Mater. Interfaces* **2021**, *13*, 14552.
[21] A. Hajalilou, A. F. Silva, P. A. Lopes, E. Parvini, C. Majidi, M. Tavakoli, *Adv. Mater. Interfaces* **2022**, *9*, 2101913.
[22] Y. Lin, C. Cooper, M. Wang, J. J. Adams, J. Genzer, M. D. Dickey, *Small* **2015**, *11*, 6397.
[23] A. Fassler, C. Majidi, *Adv. Mater.* **2015**, *27*, 1928.
[24] S. Liu, S. Y. Kim, K. E. Henry, D. S. Shah, R. Kramer-Bottiglio, *ACS Appl. Mater. Interfaces* **2021**, *13*, 28729.

© 2022 The Authors. Small published by Wiley-VCH GmbH

[25] W. Kong, Z. Wang, M. Wang, K. C. Manning, A. Uppal, M. D. Green, R. Y. Wang, K. Rykaczewski, *Adv. Mater.* **2019**, *31*, 1904309.
[26] E. J. Krings, H. Zhang, S. Sarin, J. E. Shield, S. Ryu, E. J. Markvicka, *Small* **2021**, *17*, 2104762.
[27] X. Wang, C. Lu, W. Rao, *Appl. Therm. Eng.* **2021**, *192*, 116937.
[28] H. Wang, W. Xing, S. Chen, C. Song, M. D. Dickey, T. Deng, *Adv. Mater.* **2021**, *33*, 2103104.
[29] C. Pan, D. Liu, M. J. Ford, C. Majidi, *Adv. Mater. Technol.* **2020**, *5*, 2000754.
[30] P. Wu, J. Fu, Y. Xu, Y. He, *ACS Appl. Mater. Interfaces* **2022**, *14*, 13458.
[31] S. Park, K. Mondal, R. M. Treadway III, V. Kumar, S. Ma, J. D. Holbery, M. D. Dickey, *ACS Appl. Mater. Interfaces* **2018**, *10*, 11261.
[32] J. Roth, V. Albrecht, M. Nitschke, C. Bellmann, F. Simon, S. Zschoche, S. Michel, C. Luhmann, K. Grundke, B. Voit, *Langmuir* **2008**, *24*, 12603.
[33] D. Brewis, D. Briggs, *Polymer* **1981**, *22*, 7.
[34] D. Zhang, Q. Sun, L. C. Wadsworth, *Polym. Eng. Sci.* **1998**, *38*, 965.
[35] A. M. Hubbard, W. Cui, Y. Huang, R. Takahashi, M. D. Dickey, J. Genzer, D. R. King, J. P. Gong, *Matter* **2019**, *1*, 674.
[36] L. Rossing, R. B. Scharff, B. Chömpff, C. C. Wang, E. L. Doubrovski, *Mater. Des.* **2020**, *186*, 108254.
[37] L. Xiong, P. Chen, Q. Zhou, *J. Adhes. Sci. Technol.* **2014**, *28*, 1046.
[38] S. Bhattacharya, A. Datta, J. M. Berg, S. Gangopadhyay, *J. Microelectromech. Syst.* **2005**, *14*, 590.
[39] L. A. Bloomfield, *Int. J. Adhes. Adhes.* **2016**, *68*, 239.
[40] J. Yang, A. Garton, *J. Appl. Polym. Sci.* **1993**, *48*, 359.
[41] T. Yin, G. Zhang, S. Qu, Z. Suo, *Extreme Mech. Lett.* **2021**, *46*, 101325.
[42] J. W. Krumpfer, T. J. McCarthy, *Langmuir* **2011**, *27*, 11514.
[43] H. Yuk, T. Zhang, G. A. Parada, X. Liu, X. Zhao, *Nature communications* **2016**, *7*, 1.
[44] J. M. Taylor, K. Perez-Toralla, R. Aispuro, S. A. Morin, *Adv. Mater.* **2018**, *30*, 1705333.
[45] T. An, S. Gong, Y. Ling, D. Dong, Y. Zhao, W. Cheng, *EcoMat* **2020**, *2*, e12022.
[46] T. Shen, Y. Liu, Y. Zhu, D.-Q. Yang, E. Sacher, *Appl. Surf. Sci.* **2017**, *411*, 411.
[47] A. Y. Fadeev, T. J. McCarthy, *Langmuir* **1998**, *14*, 5586.
[48] E. P. Plueddemann, *Silane Coupling Agents*, Springer, New York **1982**.
[49] A. Gent, R. Tobias, *J. Polym. Sci., Part B: Polym. Phys.* **1984**, *22*, 1483.
[50] J. Gohl, T. Thiele-Sardina, M. Rencheck, K. Erk, C. Davis, *Exp. Mech.* **2021**, *61*, 1209.
[51] N. Kazem, M. D. Bartlett, C. Majidi, *Adv. Mater.* **2018**, *30*, 1706594.
[52] S. Lee, M. Pharr, *Proc. Natl. Acad. Sci. U. S. A.* **2019**, *116*, 9251.
[53] B. Chen, D. A. Dillard, *Int. J. Adhes. Adhes.* **2001**, *21*, 357.
[54] C. Chiew, M. H. Malakooti, *Compos. Sci. Technol.* **2021**, *208*, 108752.
[55] R. W. Style, R. Tutika, J. Y. Kim, M. D. Bartlett, *Adv. Funct. Mater.* **2021**, *31*, 2005804.
[56] R. Tutika, S. H. Zhou, R. E. Napolitano, M. D. Bartlett, *Adv. Funct. Mater.* **2018**, *28*, 1804336.
[57] S. H. Jeong, S. Chen, J. Huo, E. K. Gamstedt, J. Liu, S.-L. Zhang, Z.-B. Zhang, K. Hjort, Z. Wu, *Sci. Rep.* **2015**, *5*, 18257.
[58] Y. Gao, J. Liu, *Appl. Phys. A* **2012**, *107*, 701.
[59] S. Mei, Y. Gao, Z. Deng, J. Liu, *J. Electron. Packag.* **2014**, *136*, 011009.

© 2022 The Authors. Small published by Wiley-VCH GmbH